SUBMISSION TO:

Engineering Geology

DATE:

15 Jul 2018

TITLE:

Thermal regime of permafrost at Varandey Settlement along the Barents Sea Coast, North West Arctic Russia

AUTHORS:

Thi Minh Hue Le[1,2], Ivan Depina[2], Emilie Guegan[3], Anatoly Sinitsyn[2]

AFFILIATIONS:

[1] Norwegian Geotechnical Institute, NGI, Sognsveien 72, N-0855 Oslo, Norway

[2] SINTEF Building and Infrastructure, SINTEF, Richard Birkelands vei 3, 7034 Trondheim.

Tel: +47 (0) 9300 1834; Email: thi.le@ngi.no

[3] WSP Group, Smedjegatan 24, 972 31, Luleå, Sweden.

Abstract:

Soil temperature variation is one of the governing factors of mechanical properties of frozen soils and has a large effect on the stability of soil masses in regions affected by permafrost. The understanding of the thermal regime is critical for planning, designing, constructing, and maintaining infrastructure needed to sustain communities and/or industries in these regions. Detailed studies on the effects of thermal variations based on field data measured in permafrost are limited due to the high cost and high risk associated with field investigations in these remote areas. This study will contribute to bridge the current knowledge gap through an investigation of the thermal regime in permafrost at Pesyakov Island in the Varandey settlement along the Barents Sea coast, in northwest Arctic Russia. Samples were collected and thermistor string was installed at a series of 6 boreholes along a 500 m transect. The transect crosses a coastal barrier island from the beach margin through a dune belt to the laida zone. Continuous measurement of the ground temperature over a period of two years reveals a strong correlation between the surface conditions (air temperature, vegetation, snowfall) and the variation of soil temperature above the permafrost. Numerical modelling of the transect, calibrated with the measured soil temperature, shows important features of the thermal profile, including the existence of frozen soil lenses within unfrozen soil masses and vice versa.

1   Introduction

The distribution and variation of ground temperature in permafrost soils, referred to as "thermal regime" in this study, is one of the key factors influencing soil strength. In permafrost-affected coastlines, the soil strength governs the stability of coastal bluffs where destabilized soil masses can be carried away by waves and sea currents, adding to erosion problems. Understanding of the thermal regime of these coastal areas is therefore instrumental to plan, design and construct sustainable infrastructure in such areas. This topic has become particularly important in recent decades due to increased erosion rates observed at several locations in the Arctic. Some of the most dramatic losses have been observed along the coasts of the Laptev and Beaufort Seas (Fritz et al., 2017) and in the area of Varandey settlement on the coast of the Barents Sea, in northwest Russia (Novikov and Fedorova, 1989; Guégan et al., 2016; Sinitsyn et al., 2017). This study will focus on the thermal regime of Pesyakov Island, one of the three geographical sectors of the Varandey coastline.

The Varandey region is located in northwest Russia on the shore of the Barents Sea (Fig. 1). Interests in the region have risen strongly over the years following the establishment of a key oil and gas development. The 90 km coastline, from Pesyakov Island in the southwest to the Medynskiy Zavorot Cape in the northeast, is underlain by permafrost. The coastline of the Varandey area also suffers from erosion, which has accelerated over the years at the central and north-eastern sectors due to climate change and human activities (Ogorodov, 2005; Sinitsyn et al., 2017). Pesyakov Island experiences local erosion in separate areas within its coastline, but over the last 50 years is on average relatively stable (Sinitsyn et al., 2017).

Decreasing extent and duration of sea ice that protects the coasts, and increasing air temperatures caused by global warming can lead to an increase in the rate of coastal erosion in permafrost-affected coastlines (Jones et al., 2009). It is believed that these factors can

potentially accelerate the rate of erosion on Pesyakov Island in the future, similar to the current situation of the other arctic coastlines, which are all composed from loose/Quaternary sediment. The threat to the oil and gas infrastructure due to coastline erosion stimulates special interest in the thermal regime of the soils in the Varandey settlement. There have been a limited number of published studies that contain information about the permafrost conditions at this site (e.g. Novikov and Fedorova, 1989; Ogorodov, 2004; Ogorodov, 2005; Ivanova et al., 2008; Guégan et al., 2016; Sinitsyn et al., 2017). These studies focused on the geomorphological and geocryological conditions and erosion rates at Varandey. Some studies reported limited field measurement of soil temperatures using thermistor strings (Ivanova et al., 2008; Guégan et al., 2016).

This paper focuses specifically on the thermal regime of Pesyakov Island using field measurements and numerical modelling. Long-term monitoring of ground temperature in permafrost-affected areas is often performed by deploying a thermistor string in a borehole to record the ground temperature over time. Thermistor strings are specially designed to operate under extreme temperature conditions, and have been used frequently for monitoring roads, embankments and pipelines in regions with permafrost (Heuer et al., 1982; Goering, 2003; Kristensen et al., 2008; Flynn et al., 2016; Guégan and Christiansen, 2016).

Soil temperature measured by thermistor strings is limited in time and space. It is therefore quite often supplemented with numerical modelling to extrapolate in space and time. Many studies have demonstrated the potential of numerical models to compliment field temperature data e.g., (Goering, 2003; Kristensen et al., 2008; Flynn et al., 2016). Numerical models can be used as a tool to predict thickness of the active layer and soil temperatures in permafrost. The active layer refers to the relative thin surface ground layer above the permanently cryotic soil. The active layer undergoes freezing and thawing every season. Predictions of active layer thickness and soil temperature can be utilized in designing foundations, pavements, buried

pipelines, pipeline crossings in coastal zones, and other infrastructure. The object of this study is to combine field investigation and numerical modelling to reconstruct the thermal regime of Pesyakov Island (Fig.1).
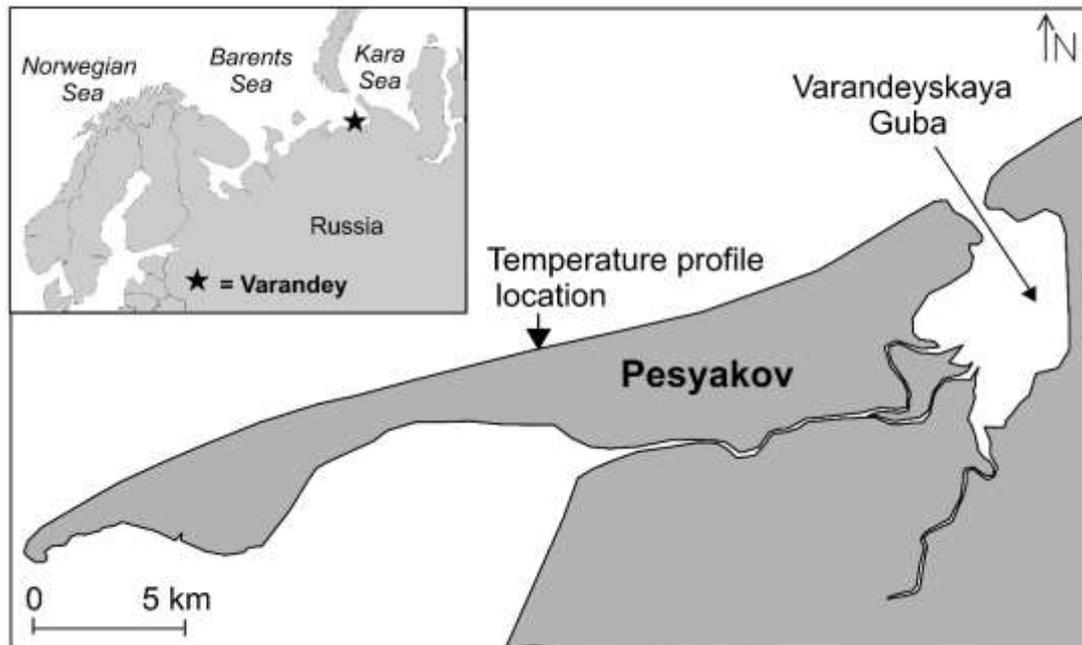

Figure 1: Map of the Pesyakov Island (main figure) at the Varandey site and location of the Varandey site in a map of northern Europe and Russia (sub-figure).

Pesyakov Island is a coastal barrier island about 33 km long, with a spit of 350 m attached to the western end (Fig. 1). The island was formed by cross-flow of fine sand from submarine coastal slopes during the period of climatic optimum (i.e. warm period) at the final stage of the Holocene transgression (Ogorodov et al., 2014). The topsoil layers are therefore characterised by relatively homogeneous medium to fine sands. Mixed organic grass remains and peaty materials can be found in soil samples at distances of more than 100 m inland from the beach. A typical cross-section of Pesyakov Island, from the beach to the lagoon, is shown in Figure 2. The cross-section is perpendicular to the coast and can be subdivided into four parts: beach, dune belt, barrier and laida (i.e. coastal wetland formed behind the barrier terrace), listed from the coast moving inland (Fig. 2). These parts are relatively distinct in geological and

geomorphological characteristics. The beach is covered with well-washed medium to fine sands with some pebbles, gravels, fragmented rock debris and single bivalve shells. The beach ranges between 80 and 100 m wide, bordered by the dune belt separating the beach from the barriers and the laida (Fig. 2). The dune belt is formed by numerous sand dunes, which lie adjacent to the beach and parallel to the coastline. The sand dunes of aeolian-marine genesis are composed of fine-grained sands and devoid of any pebbles, gravel and other coarse-grained materials. The dune width is in the order of tens of meters while the dune height is around 5 to 12 m relative to the sea level.

The relatively flat and wide barrier lies adjacent to the dune belt. The barrier is between 3 and 8 m high relative to sea level. The barrier materials consist of fine sand with some grass remains and appear to have increasing organic content with depth. The laida deposits formed under the influence of storm surges and consist of swampy areas up to 3.5 m above sea level. The laida deposits are characterised by fine sands with an abundance of grass remains and/or interbedded with thin layers of peaty organic materials. The laida can be separated into two morphological levels: upper laida corresponding to wind surges of sporadic catastrophic events (i.e., storms) and lower laida corresponding to fair weather conditions.
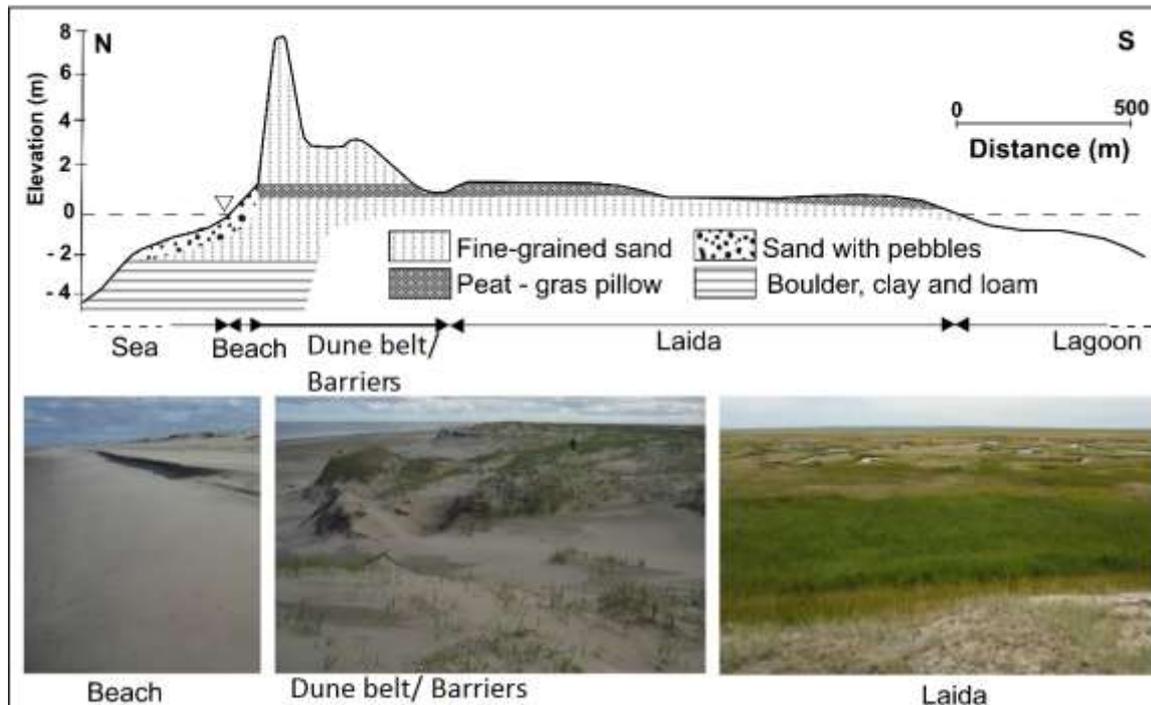
Figure 2: Schematic representation of a typical cross-section showing different morphological parts on Pesyakov Island (top figure), and pictures of the ground surface and topsoil at the beach, the dune belt and the laida (bottom sub-figures).

2 Methods

A soil investigation was carried out around the middle of the summer in two consecutive years (3–20 July 2012 and 9–16 August 2013).

2.1 Borehole drilling

Boreholes with depths ranging from 3 to 10 m were drilled at nine locations along an approximately 500 m long cross-section perpendicular to the shoreline. The cross-section is located close to the middle of the island. The drilling work was performed with a UKB 12/25 portable rig that consists of a petrol engine mounted on a collapsible metal frame. In most boreholes an auger was employed to drill through the active layer first, followed by the retrieval of ice-bonded frozen cores with a conventional (single-tube) core sampler. The sampler was able to retrieve ice-bonded sand sediments, but no sand sediment unbonded by ground ice (either noncryotic, thawed, or unfrozen)(Harris et al., 1988) could be sampled. On the dune belt, the active layer was thick and the core sampler could not grab the thawed core. Drilling was

therefore only performed with the auger. Across the studied site, the resistance to drilling was relatively constant within the active layer, but increased significantly once the ice-bonded frozen ground was reached.

At the beach, drilling with a section of auger attached to a set of drilling rods was used in an attempt to reach the active layer that was expected to be present at large depth. Due to the high salinity in the pore water, the freezing temperature of soil at the beach can drop below zero. There can therefore exist cryotic but unfrozen soils (i.e., soils or rocks at temperatures of 0°C or lower but not containing any ice) which extend below the active layer and probably turns into ice-bonded cryotic soil at very large depth.

The samples retrieved from both coring and auger drilling were used to determine grain size distribution and the gravimetric water content with soil laboratory tests. Once the boreholes were completed, thermistor strings were deployed in six selected boreholes in order to monitor the ground thermal regime across the studied area.

2.2 Thermistor string installation and measuring active layer thickness

Six thermistor strings (GEOPRECISION GmbH, 2016) were installed in six of the nine boreholes (BH) as specified in Table 1. The locations of the six boreholes with thermistor strings are indicated in Figure 3. The thermistor strings monitor the soil temperature at various locations from the upper laida (BH1 in Fig. 3) to the toe of the dune belt on the beach (BH6 in Fig. 3). The barrier and the laida are relatively flat, hence the heat transfer process occurs predominantly in the vertical direction instead of the horizontal direction. Conversely, the considerable variation of ground elevation at and near the dune belts implies that the heat transfer process occurs in both the horizontal and vertical directions. Therefore, the thermistor strings were installed closer together on the dune belt than on the barrier and the laida (Fig. 3).

Table 1: Location and depth of boreholes and thermistor strings

Borehole	Distance from the sea (m)	Borehole depth (m)	Thermistor string length (m)	Geomorphologic position	Surface cover (Aug 2012)
BH1	500	5.8	5	Upper laida	Relatively dense small grass
BH2	340	2.7	2.3	Flat sandy surface of the coastal barrier	Some small grass
BH3	260	5.5	4	Flat sandy surface of the coastal barrier	Some small grass
BH4	170	4	3	Surge berm, top of the dune belt	Some small grass
BH5	115	8	6.5	Regular berm, small coastal ridge	No surface cover
BH6	105	5.8	3.25	Bottom of the coastal bluff, top of the surge berm	No surface cover

Each thermistor string consisted of 20 individual temperature sensors with an accuracy of +/- 0.05°C and a logger. The thermistor strings were installed inside 50 mm diameter plastic casings filled with dry sand. Installation was conducted in August 2012 while the field was relative dry and warm. The air temperature was between 10 and 20°C. The casing was composed from plastic pipes with socket connections and closed with caps at both ends to protect the thermistor strings from water (e.g., thawed ice from the active layer or water in unfrozen soil lenses). The temperature log must be read at the installed location, and was retrieved three times in the period from August 2012 to Aug 2014. Temperature measurements were recorded every 3 hours for the thermistor strings near the beach area (BH4, BH5 and BH6) and every 6 hours for those located further inlands (BH1, BH2 and BH3). Logging at 10 minute intervals was also performed for all six thermistor strings over a period of 2 days (11 and 12 August 2013). The frequent logging aimed to investigate the effect of tidal fluctuation on the groundwater, and subsequently on the soil temperature at the studied site. The results of the frequent logging indicated that the tidal effect on the soil temperature was minimal, even at BH6 which was closest to the sea (Table 1).

The thickness of the active layer is also an important factor that influences the stability of slopes in permafrost soils. The soils in the active layer are significantly weaker in the "thawed" state during the warm summer months than in the "frozen" state during the cold winter months. The

thickness of the active layer therefore governs the amount of material susceptible to various types of soil mass movements.

3   Results

3.1   Geocryological characteristics

In this study, the geological/geocryological profile of Pesyakov Island has been reconstructed from the borehole data and probing to estimate depth to the frozen ground (Fig. 3). The probe was a steel rod of 1.7 m long which was used to find the top of the frozen ground at various locations on the Pesyakov island on 7 July 2012. Note that probing is a quick, low cost and simple method to check the depth to frozen ground. It can, however, be inaccurate due to encounters with large stones, tree roots, or frozen soil lenses. The top of the permafrost coincides or is slightly deeper than the top of frozen soils detected by probing in July. The probing method is considered suitable for obtaining a large number of estimation points at the current site because the soil mass is rather homogeneous with fine sand and clay and no large trees or bushes. In addition, there are very few stones and big roots that can stop the probe and cause erroneous measurements. The depths to frozen ground from probing provide a basis for estimating the depth to the permafrost and active layers. The reconstructed profile shows consistent features with the geocryological profile for the whole of Varandey settlement presented in Ivanova et al. (2008). Ivannova et al. (2008) showed that the permafrost temperature varies between -2 and -0.3 °C within the depth from 4 to 30 m, while this study shows that the temperature at the largest depth for each thermistor string varies approximately between -1.9 °C and 0.3 °C. The positive temperatures were observed at the bottom of some boreholes which did not reach the permafrost frozen soil (Guégan et al., 2016).
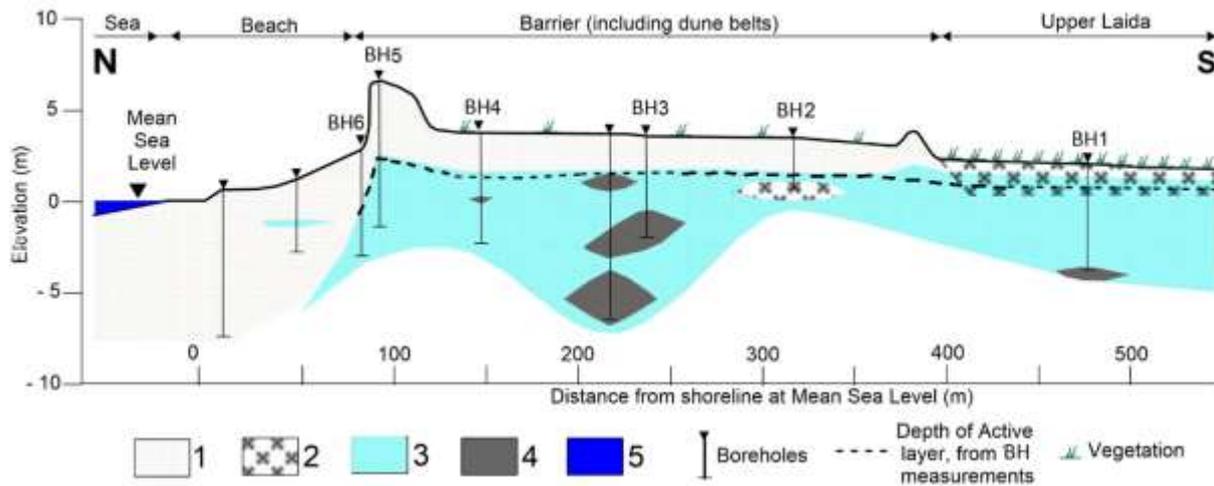
Figure 3: Interpreted geological and geocryological profile of the studied cross-section on Pesyakov island at the time of installing the thermistor strings (Aug 2012)(1) fine sand (2) sand with grass remnants (3) ice-bonded frozen ground (light blue) (4) lenses of cryopegs (5) sea water (dark blue).

The elevation of the permafrost table and the active layer thickness are estimated from the borehole profiles and thermal variation over two years of monitoring. The elevation of the permafrost table is higher beneath positive relief forms, such as on the dune belts, and then sinks to greater depth on the upper beach (Fig. 3). The average permafrost table on the barrier terrace was about 1-2 m higher than the mean sea level. The seawater temperature can be significantly higher than the air temperature in winter, and hence increases the active layer thickness on the beach. From the barrier to the beach, the active layer generally becomes thicker closer the beach (Fig. 3). The borehole data indicates that the active layer is around 2.2 m thick or more on the terrace barrier and increases to 4 m on the dune belt. On the laida, the active layer is much thinner and no longer follows the increasing trend toward the sea. The depth to frozen ground on the lower laida, measured with the permafrost probe, varies between 0.7 and 1.6 m. It then reduces to between 0.4 and 0.8 m near the boundary between the upper laida and the barrier (Fig. 3).

On the barrier terrace, lenses of frozen soil are found at depths of 1.5 and 2.2 m with thicknesses varying between 0.3 and 0.6 m. These lenses were attached to the permafrost table at some locations, while at other locations there were often layers of unfrozen highly saturated soil

interbedded between these frozen lenses and the permafrost table. These lenses were likely to be the remnants of the 'frozen' active layer which had not become fully thawed from the previous winter.

Another special geocryological feature of the permafrost at the Varandey site is the presence of cryopegs at various depths below the permafrost table. Cryopegs are layers of unfrozen ground with non-ice-cemented soils that are perennially cryotic (forming part of the permafrost). Freezing of cryopegs is prevented by freezing-point depression due to the dissolved-solids content of the pore water (Harris et al., 1988). In Pesyakov Island, the intrusion of saline pore water decreased the freezing temperature of the soils to less than zero in some parts. This led to the existence of non-ice-cemented soil lenses even though the soil temperature dropped to zero or negative values. The pore water in the cryopegs in Pesyakov Island was under higher pressure than the hydrostatic state, which raised the water column by 4.5 m on average in the boreholes where the drilling auger penetrated into these lenses. The thawed state led to difficulties in retrieving the drill columns from the boreholes with the cryopeg lenses. Boreholes where the cryopegs were found partly collapsed due to presence of saline water in the borehole. The boreholes indicated that cryopegs are present around the middle of the barrier between BH3 and BH4 (Figure 3), consistent with the description of cryopegs presented in Ivanova et al. (2008).

Another interesting feature observed during the borehole drilling was lenses of soil in a permanently frozen state under 2.2 m of the beach sediment, as shown to the left of BH6 (Figure 3). The frozen soil lenses were relatively thin and shallow, which might be the remnants of the frozen top soil layer from the last winter.

3.2 Grain size distribution and water content

Grain size analyses were performed on samples at various depths retrieved from the boreholes. The soil is composed mostly of fine sands, except for some thin peat layers found in the upper

soil horizon of the laida. The analyses were conducted using a vibrating sieve machine with a set of sieves having cell diameters of 0.045, 0.063, 0.125, 0.25, 0.1, 1, 2 and 4 mm. The range of grain size distribution (GSD) curves for various depths above seven meters from all the boreholes is indicated by the shaded area in Figure 4. For most parts of the island, the sand samples are dominated by grain sizes from 0.125 to 0.5 mm (96–99 % fraction of mass). Around 30–35 % is the 'upper' fine fraction of 0.25 to 0.5 mm and the remaining 60−65 % is of the 'lower' fine sand between 0.125 and 0.25 mm. The coarse fraction (> 2 mm) and the very fine fraction (<0.05 mm) are negligible for almost all of the samples. The narrow range of GSD curves above seven meters suggests that the site can be considered almost homogeneous for practical purposes.

The soil sample from the laida (BH2) has a higher fraction of very fine sand from 0.125 to 0.25 mm (76-82%) and a lower fraction with grain size from 0.25 to 0.5 mm (16–18%) compared with other locations.
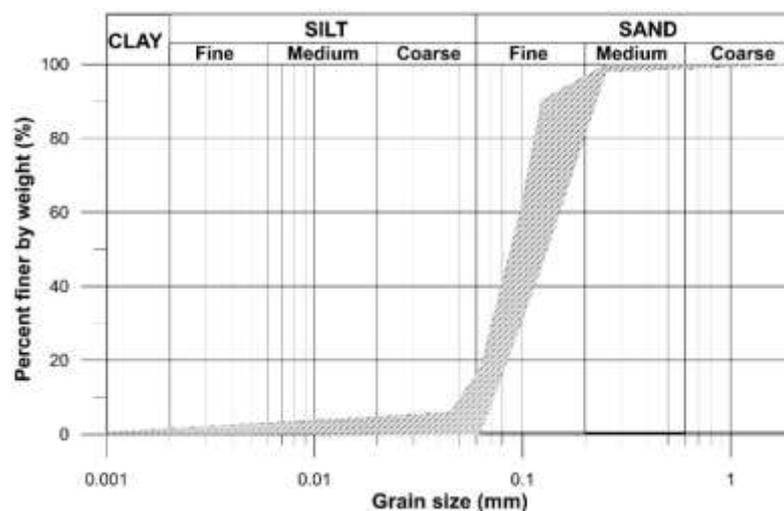

Figure 4: Grain size distribution (GSD) of soil samples from Pesyakov Island

The gravimetric water content, referred to only as 'water content' subsequently, was determined experimentally immediately after drilling and then drying in the laboratory. The water content is relatively low for most samples, ranging from 10 to 30% (Fig. 5) except at BH5. Some

samples from the upper 6 m retrieved from BH5 show very low water content, around 4-5%, which suggests that the sands on the top part of the dune belt are unsaturated. Visual observation and past experience indicates that the permafrost on the dune belt is likely to have ice content of less than 5% (i.e., ice-poor). Conversely, a sample of the saturated peat layer at 1 m depth in the laida was found to have 110% water content. Note that the peat sample is excluded from Figure 5 to avoid skewness of the figure.
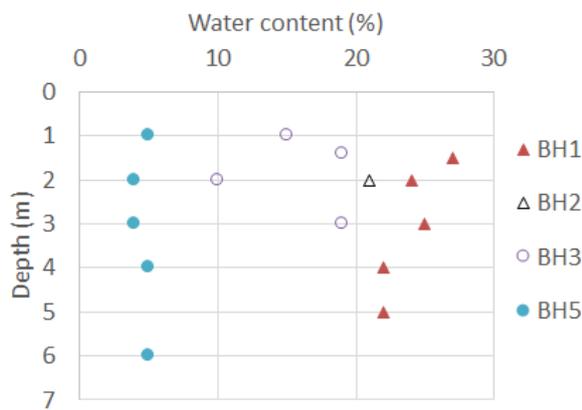

Figure 5: Water content of samples from five boreholes on Pesyakov Island

3.3 Air temperature and snow depth

A set of daily air temperatures, rainfall and snowfall were retrieved from the Varandey hydro-meteorological station on the western part of Varandey Island (Raspisaniye Pogodi Ltd., 2016). The aim is to examine the dependency of the soil temperature on these climate factors. The air temperature was measured every three hours while the amount of rainfall and snowfall (in centimeters) were measured daily at 6 am. The record showed almost no rainfall in the period of interest, hence this factor is not discussed further in this study. Figure 6 shows the variation of air temperature and accumulated snow depth over the studied period.

Both winters in the studied period were mild relative to the usual winter temperature in Varandey. The mean annual temperature was -3.8 °C in 2012–2013 and -4.8 °C in 2013–2014. The average temperatures were significantly elevated over 2-3 weeks in February 2013 and in March 2014 (Fig. 6). The elevated air temperatures during these weeks were between 0 and -5 °C, which were 20 to 30 °C warmer than the usual winter temperatures in Varandey. On average, the winter of 2012–2013 was milder than the winter of 2013–2014, while the summer 2013 was warmer than the summer 2014. The coldest air temperature was -33.5 °C on 2 March

2013 and -39.4 °C on 26 January 2014, while the warmest air temperature was 30 °C on 23 July 2013 and 20.2 °C on 1 August 2014.

The values of the air thawing index, I_{at}, and air freezing index, I_{af}, in this study are determined based on the available air temperatures and the equations suggested in Andersland and Ladanyi (2004). I_{at} is defined as the number of positive degree-days between the minimum and the following maximum on a cumulative air index curve. Conversely, I_{af} is determined as the number of negative degree-days from the maximum point to the following minimum on a cumulative air index curve (Andersland and Ladanyi, 2004). The value of I_{at} is estimated to be 1086 °C-days for 2012–2013 and 773 °C-days for 2013–2014 while the air freezing index I_{af} is -2991 °C-days for 2012–2013 and -2631 °C-days for 2013–2014. These values are typical for areas with permafrost (Andersland and Ladanyi, 2004).
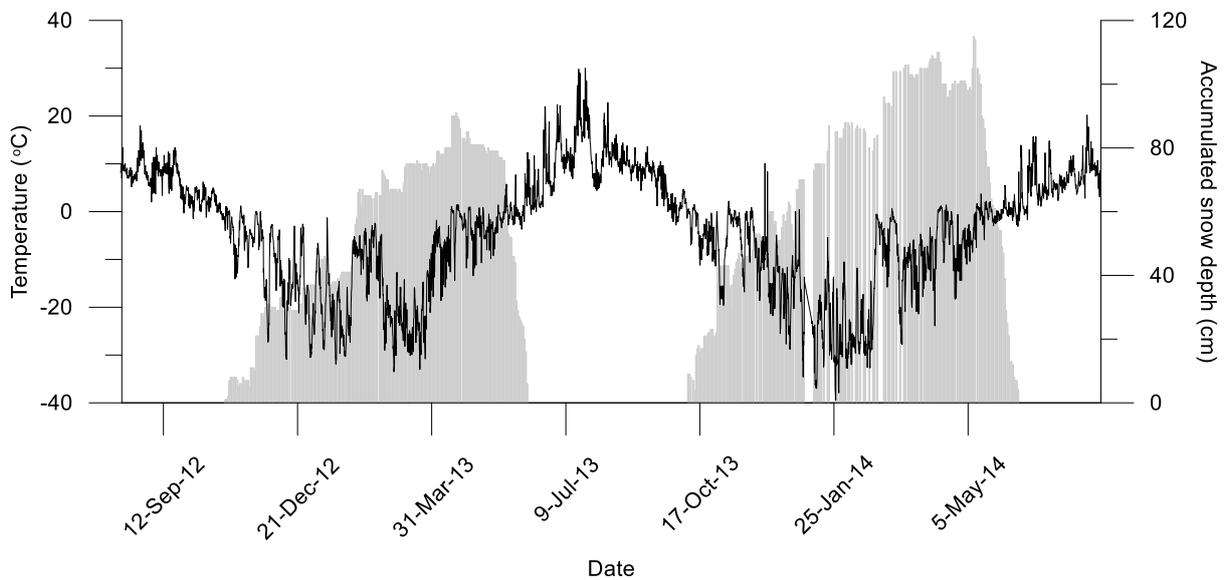

Figure 6: Variation of air temperature (continuous line) and accumulated snow depth (bar chart)

The ground surface temperature (GST) is a useful parameter indicating the condition for thermal transmission of the permafrost. The relative magnitude between the GST and the air temperature is governed by the amount of heat that can be transmitted from the air into the soil (or vice versa) through the top layers of soil, snow, grass remains, grass, scrubs and other surface covers. The GST should normally be measured within 2 cm depth (Ostercamp, 2003; Guglielmin, 2006; CALM, 2017). Such shallow measurements are, however, difficult to obtain accurately and are not available in this study. The GSTs in this study were indicative only by

considering the temperatures measured by the shallowest sensors (at depths between 25 and 50 cm) in the six boreholes installed with thermistor strings. It is important to note that there can often be a very strong gradient in temperature between the soil surface and depth in cryosol environments. The deviation between temperature at these shallowest sensors and the air temperature varies among the boreholes, which indicates that the insulating capacity of the top cover is non-uniform across the studied site. The largest deviation is observed at BH6 (at the toe of the bluffs, on the lee side of the dune belt) where the minimum temperature was above -4 °C in winter in both 2012 and 2013, even though the air temperature dropped to less than -30 °C.

3.4   Soil temperature variation

Figures 7–10 show the soil and air temperature variation against time and seasonal snapshots (at every three months) of the soil temperature against depth. In Figures 7-10a, the temperature variation decreases as the depth (shown in the legend) increases, hence the curve becomes increasingly flat with depth.

Near the sea

BH6 was located at the toe of the bluff on the beach and closest to the sea among all the boreholes (Fig. 3). The top one meter of the soil at BH6 was an aeolian deposit, underlain by a layer of yellow beach sand of around 2 m thick. Permafrost started at approximately 3.2 m depth, with a layer of frozen yellow sand from 3.2 to 3.5 m. From 3.5 m downward, the frozen sand appeared to be dark grey or blue grey in colour, with fine grains and a silt fraction.

The soil temperature variation during winter at BH6 was distinctly different from that at the other five boreholes further from the sea. Figure 7 shows that the temperature at all depths stayed almost constant between -2 °C and 0 °C during the winter months, even though the coldest air temperatures were -30 °C in winter 2012−2013 and between -30 and -40 °C in winter

2013−2014. The most prominent factors contributing to the high ground temperature in winter are the strong influence of the seawater temperature on the ground temperatures (when compared to the other boreholes) and the insulating effect of the snow bank accumulated on the coastal bluffs during winter.

The Barents Sea was one of the warmest seas in the Arctic ocean due to a large influx of warm Atlantic water. Particularly, water in the south-eastern coastline of the Barents Sea near the Varandey site is influenced by these warm currents at shallow depths (AARI, 2016). The maximum summer temperature of surface water in this area can reach 15 ℃ in the open sea and 23 ℃ in Pechora Bay, while the minimum winter surface water temperature is between zero and -1 ℃. This temperature can extend to 100 m water depth and can therefore influence the soil temperature near the coast (AARI, 2016). Since the air temperature is much lower than the seawater temperature during the winter months, the seawater can act as a heat source raising the soil temperature in the winter.

The second possible influence to the soil temperature is the snow bank. Winds blowing from the land towards the sea create a low pressure zone immediately behind the crest, which causes the snow to fall and accumulate over time. The top material of the dune belts is an aeolian deposit, which indicates that the wind effect can be significant at this location. In addition, the dune belt acts as a natural obstacle to the wind, trapping the snow, and leading to snowbank accumulation (Gubarkov et al., 2009). The thermal conductivity of loose snow on the ground is around 7–10 $kJday^{-1}m^{-1}℃^{-1}$, which is 10–20 times lower than that of the soils (Andersland and Ladanyi, 2004). Therefore, the snow bank acts as an effective thermal insulator, limiting heat loss from the ground in winter and insulating the soil underneath from the cold air.

From mid-April to mid-October, when the air temperature was above zero, the variation of the measured soil temperatures reflected quite closely the variation pattern of the air temperatures (Fig. 7). The ground temperature during summer is strongly influenced by the direct heating of

the sun due to minimal vegetation near the beach. As the depth increases, the soil temperature variation decreases in magnitude and becomes delayed in time relative to the variation of the air temperature. For example, the summer temperature peaked at around 30 ℃ on 12 July 2013, while the corresponding peak in soil temperature at 0.5 m depth was at approximately 12 ℃ eight days later.

Near the end of 2012, the first significant snow fall occurred on 20 November with accumulated snow depth of more than 20 cm (Fig. 6). The air temperature dropped below freezing for the first time on 30 October, however, it then fluctuated with some days above zero between 30 October and 20 November 2012 (Fig. 7). The ground was therefore unlikely to be fully frozen by the first significant snowfall. Some latent heat from the unfrozen soil was likely to be impeded from being dissipated into the air (i.e., 'trapped') by the accumulating snowbank. The 'trapping' of the latent heat stopped the ground from further decreasing in temperature during winter 2012−2013. Similarly, in 2013, the first day with negative air temperature was 10 October 2013, however the temperature fluctuated around 0 ℃ before the first significant snow fall occurred on 14 October (Fig. 7). The ground temperature in winter 2013−2014 was also therefore elevated due to the 'trapped' latent heat of the soil.
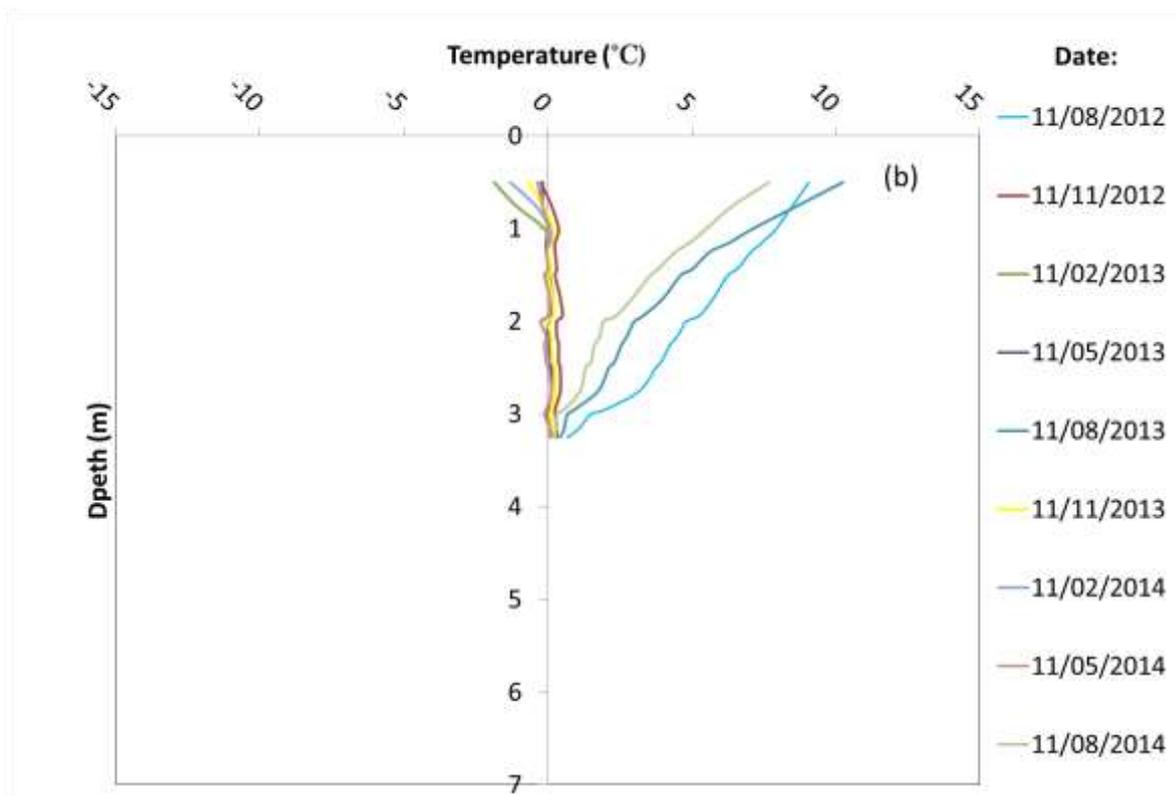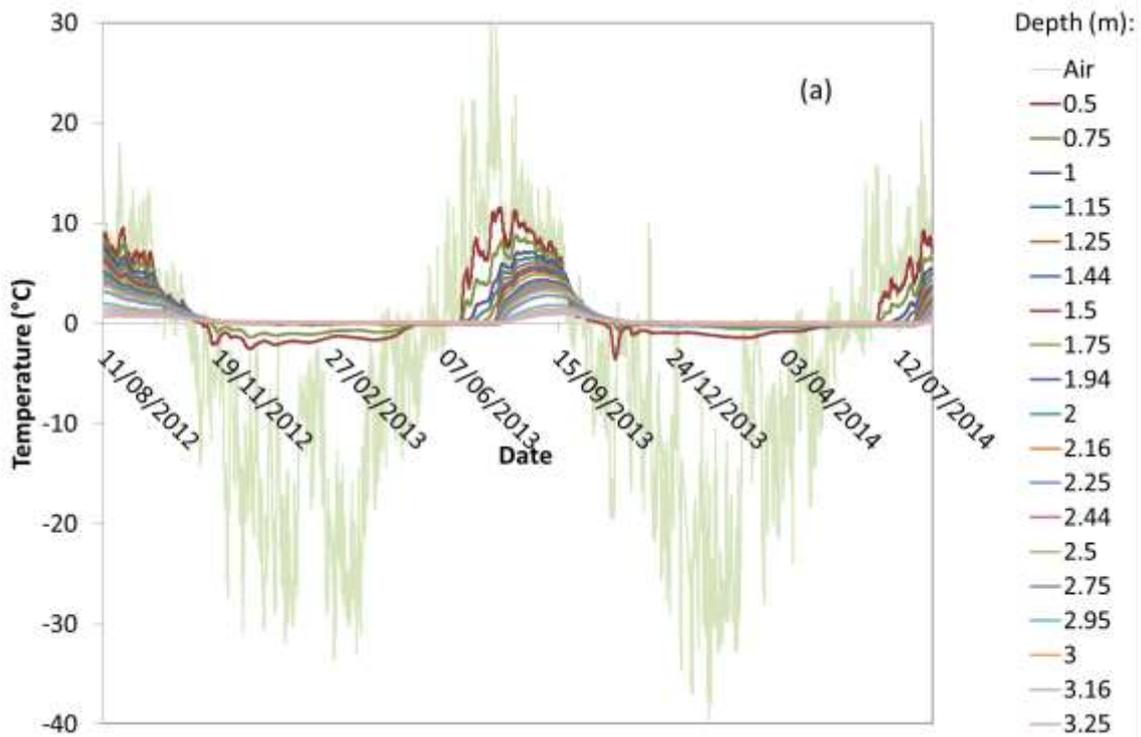
Figure 7: Variation of soil temperature at BH6 with (a) Time (the curves decrease in variation range with increasing depth) and (b) Depth.

On the dune belt

BH5 on top of the dune belt has a depth of 6.5 m (Fig. 8a). The seasonally thawed layer was approximately 4 m thick, which appeared as yellow grey fine-grained sand. Similar material was found in the next layer, between 4 and 6.6 m, which was continuously frozen in the two years studied (Fig. 8b). The dune belt sand was mostly clean with less fine materials and organic matter than at other locations. Sampling from another nearby borehole on the dune belt revealed that there might be cryopegs between 5 and 7 m underneath this area.

The top of the dune belt was likely to experience the opposite effect to that of the bluffs where the wind "eroded" the snow deposits. The snow cover on the dune belt was therefore thinner than at other locations and in some places was completely eroded. Consequently, the air temperature influenced the soil temperature more effectively on the dune belts than at other locations. In addition, the thick and uniform top sand layer had higher thermal conductivity and lower heat capacity than soils at other locations. The transmission of heat into/out of the dune belts tended to occur at a faster rate than at other locations (e.g., the laida, the barrier and the beach).

During winter, the soil temperature at 0.5 m depth on the dune belt was closer in magnitude to the air temperature than that at other boreholes (Fig. 8). It peaked at around 15 ºC when the air temperature peaked at 25−30 ºC during summers. When the air temperature dropped to the lowest, between -25 ºC and -35 ºC during winters, the soil temperature dropped correspondingly to between -15 ºC and -20 ºC after a delay of 3−8 days (Fig. 8). Interestingly, even though the coldest air temperature was lower for the winter of 2013–2014 than for the winter of 2012−2013, the soil temperatures at the same depth were several degrees higher for the winter of 2013–2014 than for the winter of 2012–2013. This could be explained by the thicker snowfall in the latter year than in the former year, observed at the weather station at Varandey (Fig. 6), which provided a more efficient insulating layer to the soils. The results show that the

proportion of heat emitted from or absorbed in the soils varies on a seasonal and annual basis. It depends on the complex combined effect of climatic variables (e.g., temperature, snow depth, wind, vegetation), and geological and geomorphological factors (e.g., soil materials, locations). This must be taken into account in further synthesizing of the data, for example, in numerical modelling or building/construction work at the site.
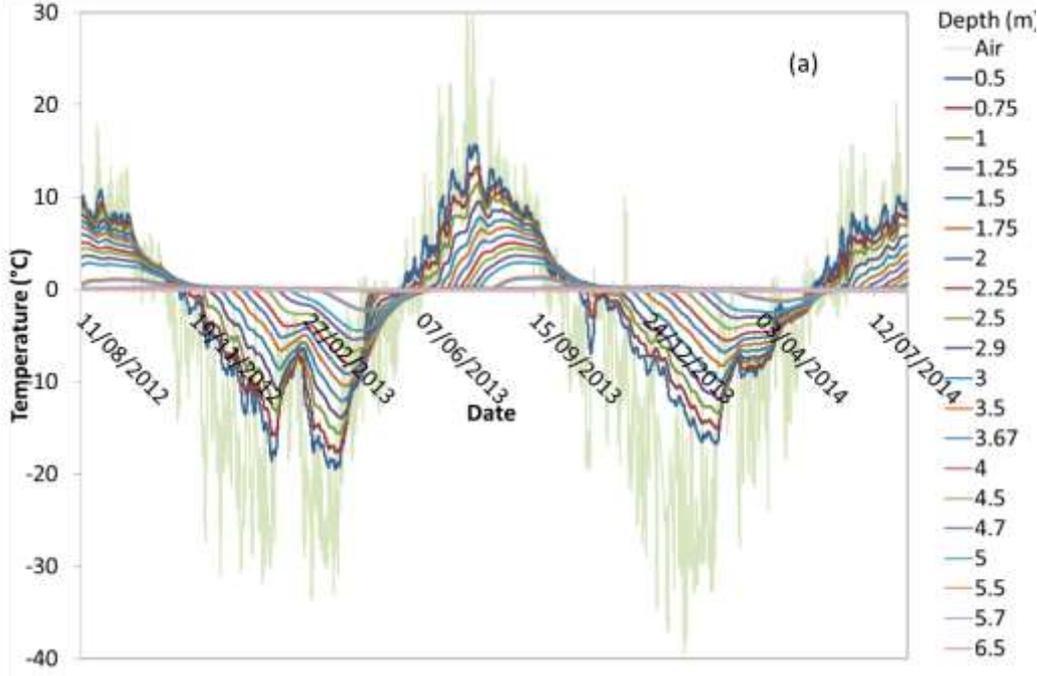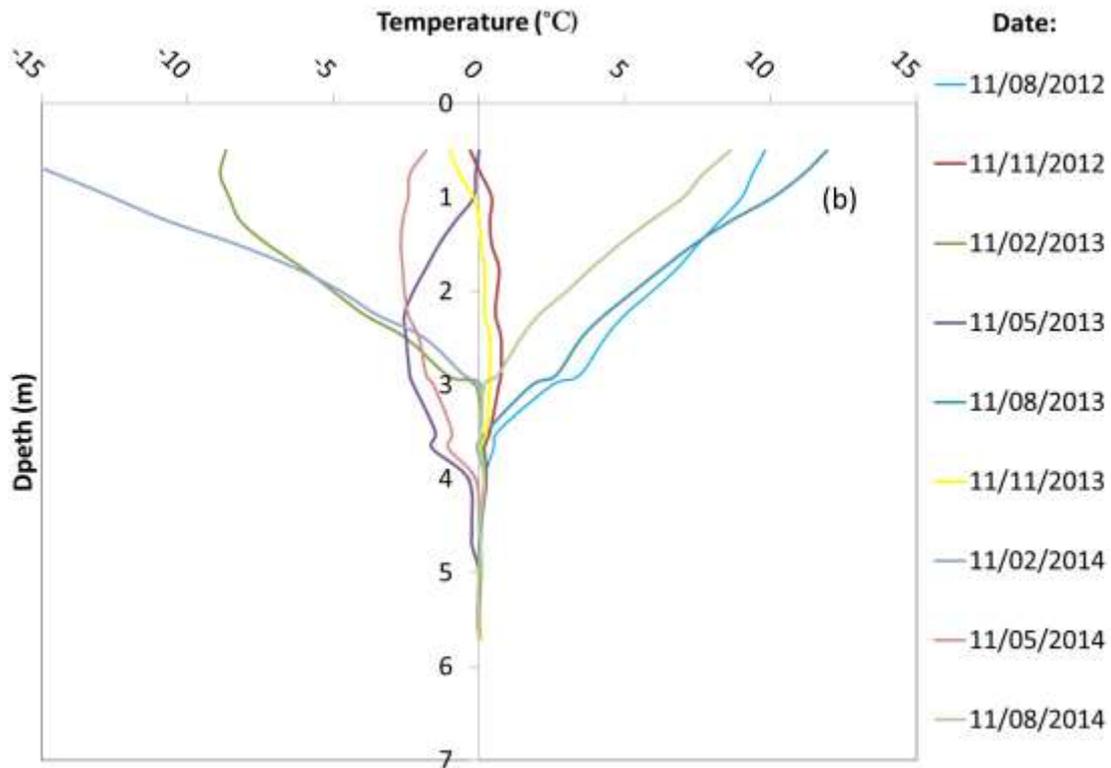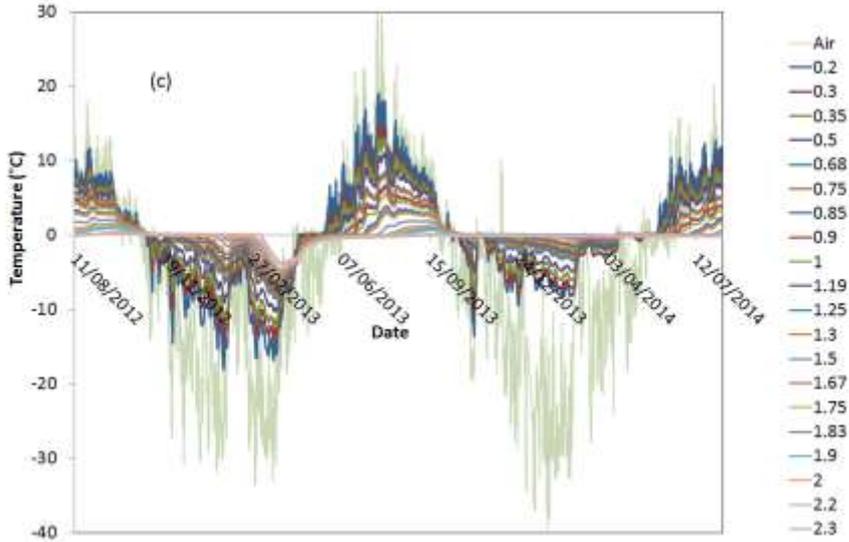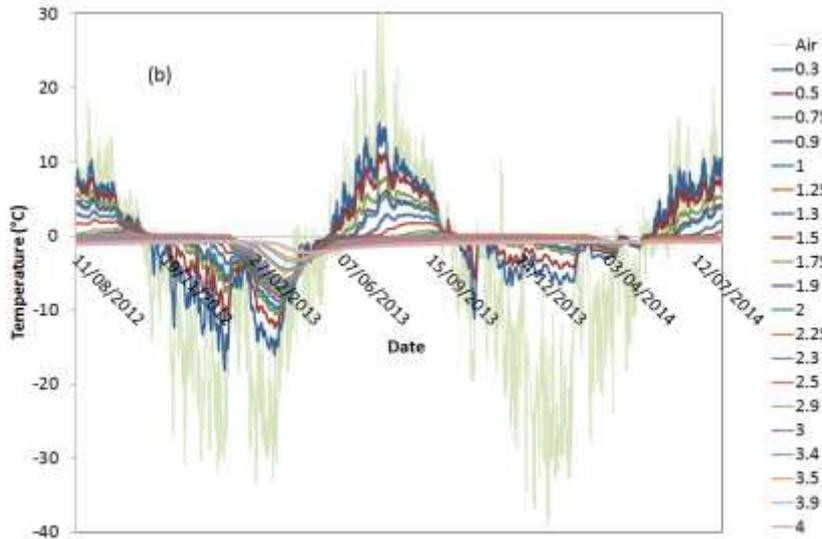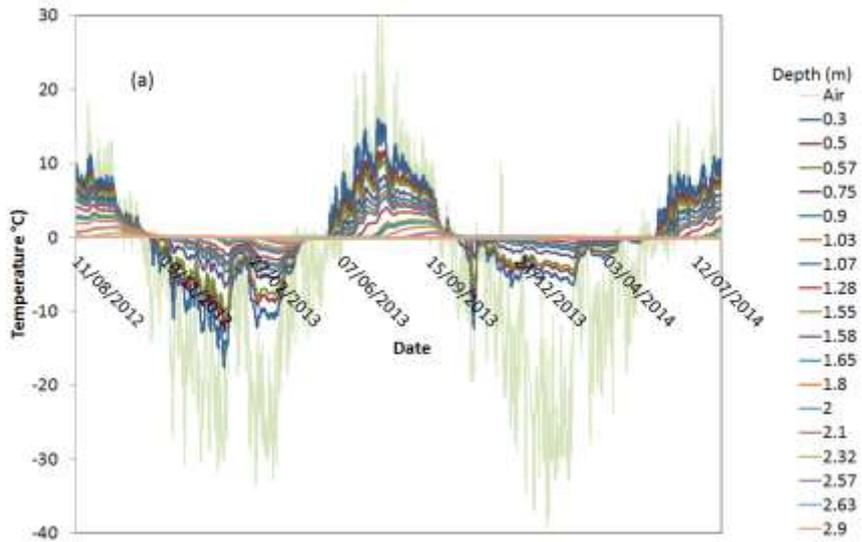
Figure 8: Variation of soil temperature at BH5 with (a) Time (the curves decrease in variation range with increasing depth) and (b) Depth.

On the barrier

The soil temperatures at three boreholes (BH2-4) on the barrier varied in a similar pattern to each other and reflected the air temperature variation with a delay of 3−8 days (Fig. 9a). Between 0.25 and 0.5 m depth, the lowest soil temperature in the winter of 2012−2013 was approximately -18 ℃, higher than that on the dune belt (-20 ℃), but lower than that on the bluff (-2.5 ℃). This can be attributed to thicker snow cover on the barrier than on the dune belt, but thinner than on the bluff. In addition, the barrier top soils were likely to contain more organic and fine materials with a higher moisture content than the dune belt sands, leading to lower thermal conductivity and higher heat capacity.

Similar to the observations on the bluff, the thinner snow cover in winter 2012−2013 than in 2013–2014 coincided with lower soil temperatures in the former than the latter year despite the higher air temperature (Fig. 9).
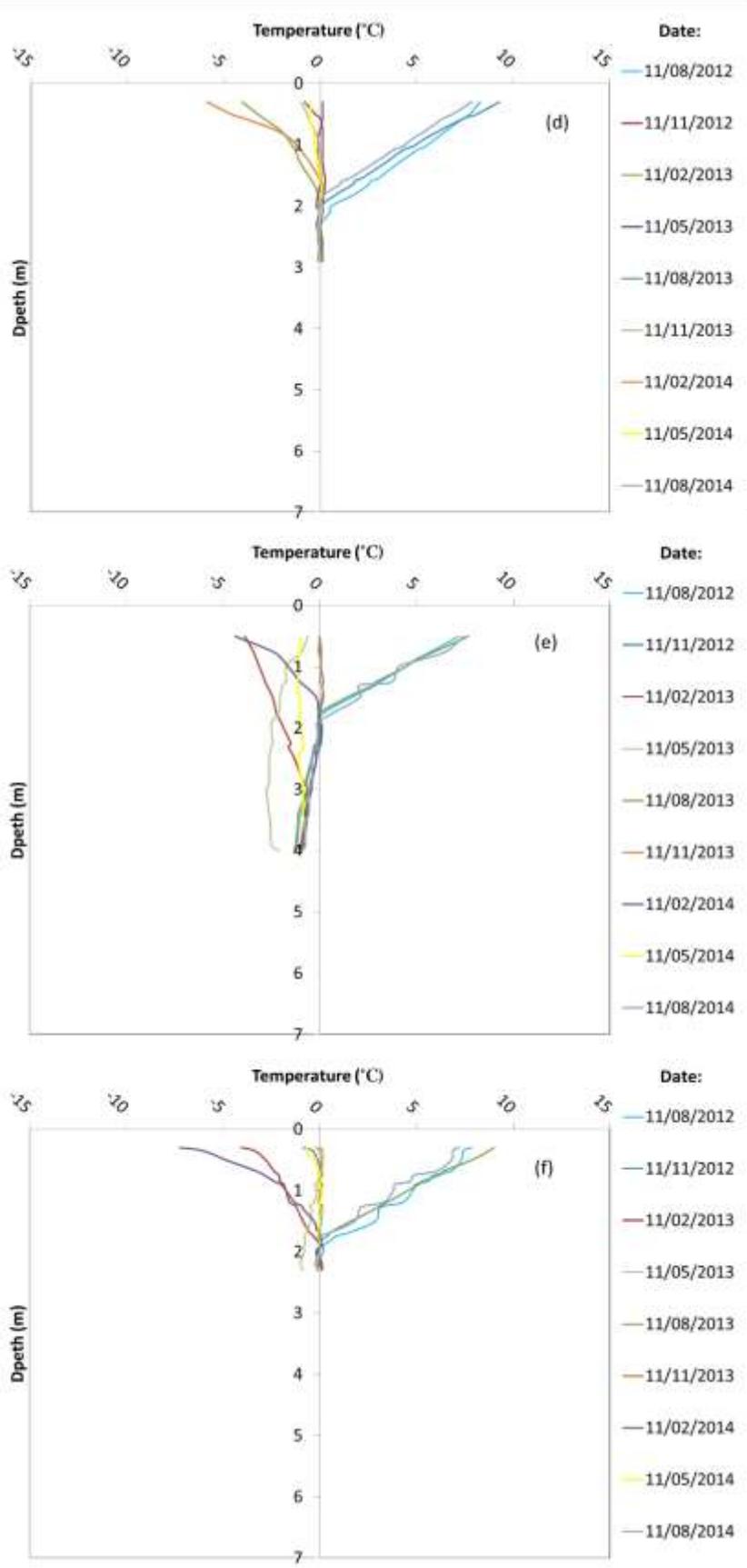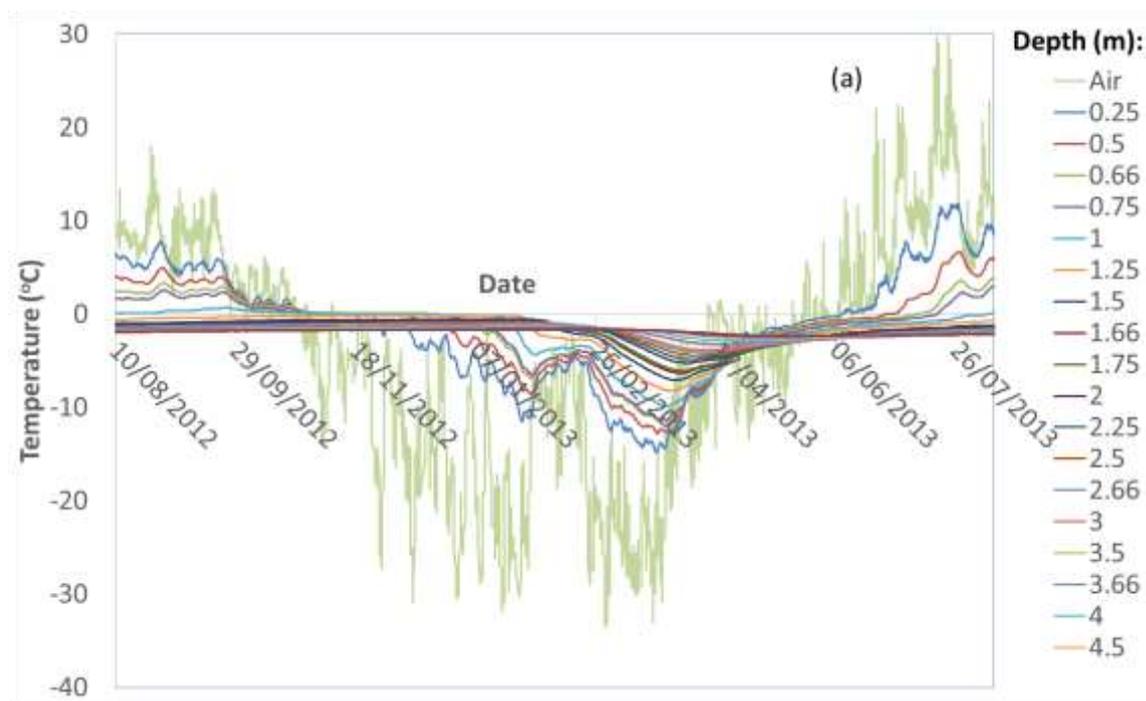
Figure 9: Variation of soil temperature at (a, d) BH4, (b, e) BH3 and (c, f) BH2 with (a, b, c) Time (the curves decrease in variation range with increasing depth) and (d, e, f) Depth.

24

Upper laida

This borehole (BH1) was located the farthest inland among all of the boreholes (almost 500 m from the beach) and has the thickest grass cover. At this location, a thick layer of silty sand (~ 5.6 m) was found overlaying fine sand in which the borehole stops. Soil temperature data could only be retrieved for the period from August 2012 to August 2013 at this borehole because the thermistor string was damaged by frost heave in the winter of 2013. The variation of the measured soil temperature on the upper laida (Fig. 10) was quite similar to that on the barrier (Fig.9). At 0.5 m depth, the lowest soil temperature was around -15 ℃ in the winter 2012–2013, which was higher than on the barrier. This might be explained by the extra insulation provided by the thicker grass cover on the laida than on the barrier.
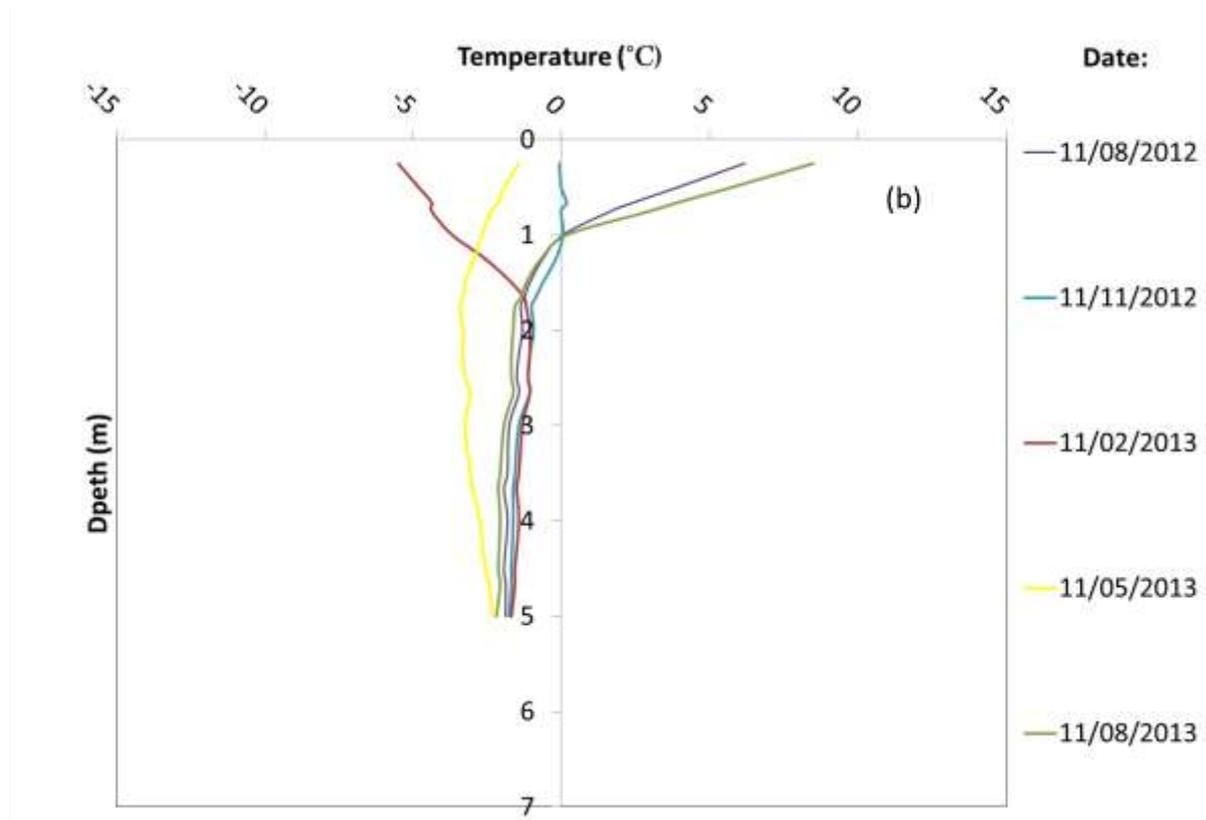
Figure 10: Variation of soil temperature at BH1 with (a) Time (the curves decrease in variation range with increasing depth) and (b) Depth.

3.5 Numerical modelling

For engineering applications in permafrost, predicting the thickness of the active layer is a key task because soils in a thawed state have a lower strength compared with soils in a frozen state. This reduction leads to instability, settlement and erosion problems when constructing infrastructure on or in active layers.

The long continuous records of ground temperature measurements provide a valuable opportunity to construct and calibrate a numerical model to analyse the thermal regime of the Varandey site. Such a model can be used, for example, to predict the regional thermal variation for designing infrastructure in the region. This study employs the finite element method by using a commercial software TEMP/W (GEO-SLOPE, 2012) to simulate the soil temperature

variation over the monitored two-year period. Even though hydrological (e.g., ground water flow) and mechanical processes (e.g., compression of the ground due to snow loading) might also influence heat flow besides the thermal processes, there is little information from the field investigation indicating the significance of these processes. Therefore, only the thermal processes are taken into account in this study while the hydrological and mechanical processes are not included. In modelling the thermal processes, only heat transferred by conduction is included while heat transferred by convection and radiation are ignored due to the limitation of the available software and the lack of data to support a more advanced model.

Among the six boreholes with installed thermistor strings, BH1, BH2 and BH3 are located furthest from the coast on relatively flat terrain (Fig. 3). This suggests that heat flow at these locations tend to conduct vertically. In addition, these three boreholes are located at rather large distances from one another, between 100 and 150 m, and hence the data from one borehole gives little information about the thermal and soil conditions at other boreholes. One-dimensional (1D) models are therefore selected for these three boreholes and considered to be adequate to capture the thermal conduction process. Conversely, BH4, BH5 and BH6 are located in an area having more complex terrain, with features such as dune belts, bluffs and beach. This area is adjacent to the sea, which can act as a heat source or sink. Therefore, a two-dimensional (2D) model is necessary to describe the heat flow in both the vertical and horizontal directions (Fig. 11).

The soils found on Pesyakov Island are categorised into different types as presented in Table 2 based on the observation in the field and test results from the laboratory. The properties corresponding to each soil type in Table 2 are shown in Table 3. These parameter values were used as an input to the numerical models of the thermal variation at the site. Table 4 shows the estimated depth and thickness of different soil layers in the boreholes. Note that the three layers in the 2D model for BH4, BH5 and BH6 have varying thicknesses.

In Table 4, the gravimetric water content (w_g) was measured for a number of samples taken from the site, while the dry densities (ρ_d) were not directly measured. The values of ρ_d selected for simulation, shown in Table 3, are based on typical ρ_d values for each soil type (ASABE, 2017). The water density (ρ_w=1000 kg/m^3) and the solid particle density (ρ_s=2650 kg/m^3) are assumed to be constant. The volumetric water content (w_θ) is estimated from the relationship with gravimetric water content, $w_\theta = w_g \cdot \rho_d/\rho_w$. The void ratio ($e$) is also estimated from the relationship with solid and dry densities, $e = \rho_s/\rho_d$-1. The volumetric heat capacity of water (c_w=4.19 kJkg$^{-1\text{o}}$C^{-1}) and ice (c_i=2.09 kJkg$^{-1\text{o}}$C^{-1}) are adapted from the values given in Andersland and Ladanyi (2004). The volumetric heat capacity of soil particles is assumed to be typical of quartz for most soils (c_s=0.73 kJ/kg.$^\text{o}$C). If a soil has a significant component of peat or plant residues, the c_s is set at a slightly higher value (0.8 and 1.0 kJ/kg.$^\text{o}$C)(Table 4). The frozen (C_f) and unfrozen (C_u) volumetric heat capacities of soil are calculated using the relations $C_f = \rho_d.(c_s + c_iw_g)$ and $C_u = \rho_d.(c_s + c_ww_g)$. The unfrozen ($k_u$) and frozen ($k_f$) thermal conductivities are estimated using equations for coarse-grained soils, with less than 20% silt-clay content (Kersten, 1949; Farouki, 1981):

$k_u = 0.1442(0.7\log w + 0.4)10^{0.6243\rho d}$

$k_f = 0.01096.10^{0.8116\rho d} + 0.00461.10^{0.9115\rho d}w$

where w is the water content (%) and ρ_d is the dry density (g/cm^3)

Table 2: Description of different soil layers found on Pesyakov Island

Soil layers	Abbreviation	Descriptions
Clean SAND	S	well washed sand
Loamy SAND	LS	loamy sand with some plant residues
Sandy PEAT	P	peat with some interbedded sand
Silty SAND 1	SS1	grey silt with fine sand
Silty SAND 2	SS2	black peaty silty medium - fine sand
Silty SAND 3	SS3	blue grey silty fine sand with some plant residues
Peaty SAND	PS	peaty iron-brown sand
CRYOPEGS	C	non-ice-cemented soil saturated with saline pore water

Table 3: Soil parameters used in the numerical models (see Table 2 for abbreviations for soil layers and soil descriptions)

Parameters	Units	S	LS	P	SS1	SS2	SS3	PS	C
w_g	%	15	23	112	30	25	23	27	25
w_θ	%	23	29	56	44	36	33	38	36
ρ_d	kg/m^3	1500	1280	500	1450	1450	1450	1400	1450
ρ	kg/m^3	1725	1574	1060	1885	1813	1784	1778	1813
e		0.77	1.07	4.30	0.83	0.83	0.83	0.89	0.83
c_s	kJ/kg^{o}C	0.73	0.73	1.00	0.73	0.73	0.80	1.00	0.71
C_u	kJ/(m$^{3.o}$C)	2038	2168	2846	2881	2577	2557	2984	2548
C_f	kJ/(m$^{3.o}$C)	1565	1550	1670	1968	1816	1857	2190	1787
k_u	kJ / (day·m·^{o}C)	136	109	47	149	143	140	135	143
k_f	kJ / (day·m·^{o}C)	155	145	130	265	223	206	216	223

Table 4: Soil types and thickness at each boreholes (see Table 2 for abbreviations for soil layers and soil descriptions)

BH1		BH2		BH3	
Depth (m)	Soil type	Depth (m)	Soil type	Depth (m)	Soil type
0–0.3	LS	0–1.5	SS2	0–1.3	SS3
0.3–0.4	P	1.5–2.7	PS	1.3–4	CS
0.4–0.6	SS1	2.5–2.7	SS1	4–5.5	C
0.6–1.2	SS2	**BH4 - BH5 - BH6**			
1.2–1.75	PS	Depth (m)	Soil type	Thickness (m)	Note
1.75–5.6	SS3	1–7	LS	1–7	thickness varies
5.6–5.8	C	1–8	SS2	1–6	thickness varies
		10–17	SS3	2–8	thickness varies

The "full thermal model" option (in TEMP/W) is selected for all the soil materials, which implies that both the unfrozen water content and the thermal conductivity vary with temperature. These dependencies were not measured for the soils in Varandey, hence the typical functions for similar soil types are adapted from those suggested in the TEMP/W manual (GEO-SLOPE, 2012).

An important element which must be taken into account in the numerical models is the difference between the mean annual ground surface temperature (GST) and the mean annual air temperature at each specific location. Some factors that contribute to this difference include vegetation, snow cover, direct heating from solar radiation where ground cover is minimal,

thermal property of the topsoil, surface relief and drainage condition. In TEMP/W, this difference is represented by an n_{factor}, which is a scale that relates the GST to the air temperature. In this study, the n_{factor} at each location is estimated by a parametric study. The selected n_{factor} is the value that can best reproduce the temperature variation obtained at the shallowest thermistors. The value of n_{factor} is different for each section because of differences in surface cover and topsoil conditions. Table 5 shows the n_{factor} for BH1, BH2, BH3 and different sections of the upper boundary of the 2D model (Fig. 11).

Table 5: The values of n_{factor} used in the numerical models

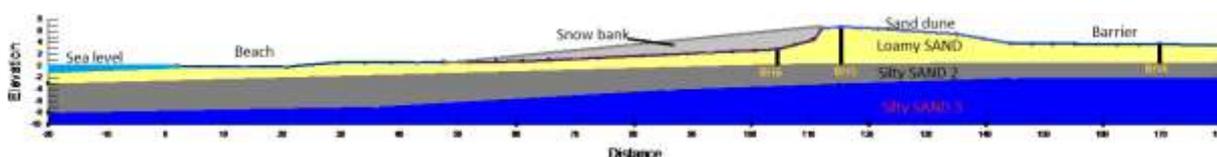| Upper boundary	2012−2013		2013−2014	
	n_{freeze}	n_{thaw}	n_{freeze}	n_{thaw}
BH1	0.5	0.6		
BH2	0.5	1	0.2	1
BH3	0.6	1	0.2	1.5
Beach	0.4	1.3	0.4	1.3
Barrier and Laida (BH4)	0.4	1.3	0.4	1.3
Sand dune (BH5)	1	2	1	2
Snowbank (BH6)	0.1	1.2	0.1	1.3

Figure 11: 2D model of the cross-section including BH4, BH5 and BH6, from the beach to the barrier

In the 2D model (Fig. 11), the 'seawater' boundary is imposed for the upper left boundary (between x = -20 and x = 0). The seawater temperature is varied smoothly between the maximum value of 20 ºC in summer and the minimum value -1 ºC in winter following a sinusoidal function. The snowbank is modelled by selecting a very low n_{freeze} factor to represent the insulating effect (Table 4). The actual snowbank mass and seawater mass are not included in the model.

The top boundary, from the beach to the barrier, is imposed with the air temperature. The bottom boundary, from x= 40 and inland, is assumed to be fixed at -1 °C, which is equal to the average

constant temperature of permafrost. From x = 40 towards the sea, the bottom boundary temperature is assumed to increase at a constant low gradient, by 0.5 °C every 10 m.
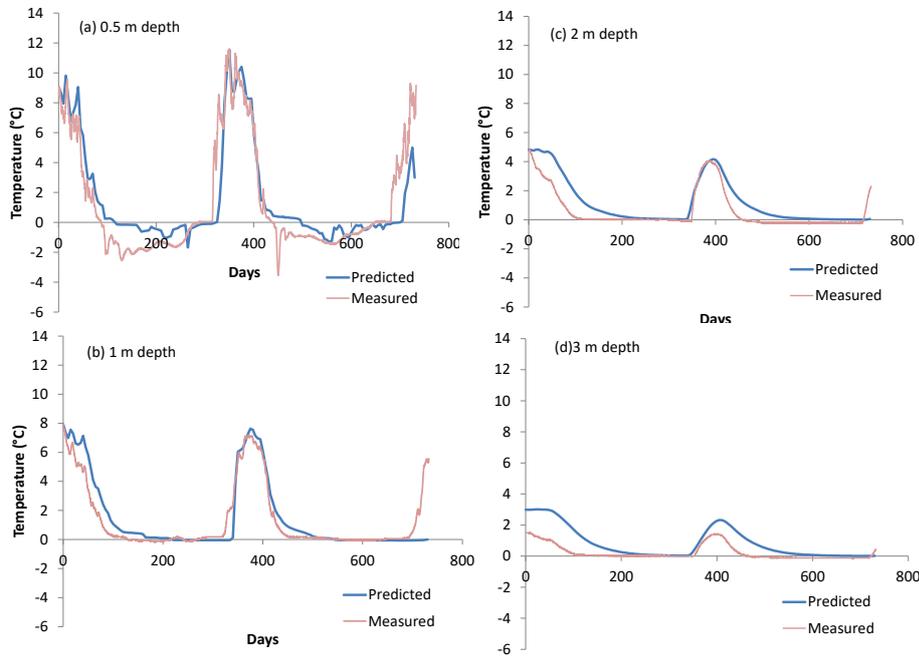

Figure 12: Comparison between measured and predicted variation of temperature at 4 different depths in BH6. Horizontal axis show the number of days from the initial date (12 Aug 2012).

Figure 12 compares the variation of soil temperature at four different depths with the predicted value by the numerical model. The 2D predicted values show good agreement with the measured temperature, though the differences between them increases over time and with increasing depth. This trend is generally expected since the initial time is set as initial conditions, and the ground surface is set as the boundary condition.

Seasonal snapshots of predicted temperature distribution are shown in Figure 13, which demonstrate the capability of the model to reproduce complex thermal evolution over time. The isolines at zero degree show the boundary between frozen and unfrozen soils. An interesting observation from the 2D model is the formation of frozen soil lenses within the unfrozen top soil and unfrozen soil lenses within the frozen masses. When the air temperature drops (i.e. transition from summer to winter), the frozen front migrating down might not completely meet

the permafrost table from the previous year. The unfrozen soil lenses can therefore form within frozen soil masses (see mid-summer 2013, Fig. 13), which might cause over-estimation of the soil strength in winter. Conversely, there might be remnant frozen soil lenses within the unfrozen soil masses (see mid-summer 2013, Fig. 13) because the soils have not completely thawed during summer. These frozen soil lenses might be mistakenly taken to be the top of the permafrost table if drilling does not go through these lenses/layers. These features observed from the 2D numerical model demonstrate the potential of the numerical method to compliment the information from soil investigation to increase understanding of the complex thermal regime in permafrost.
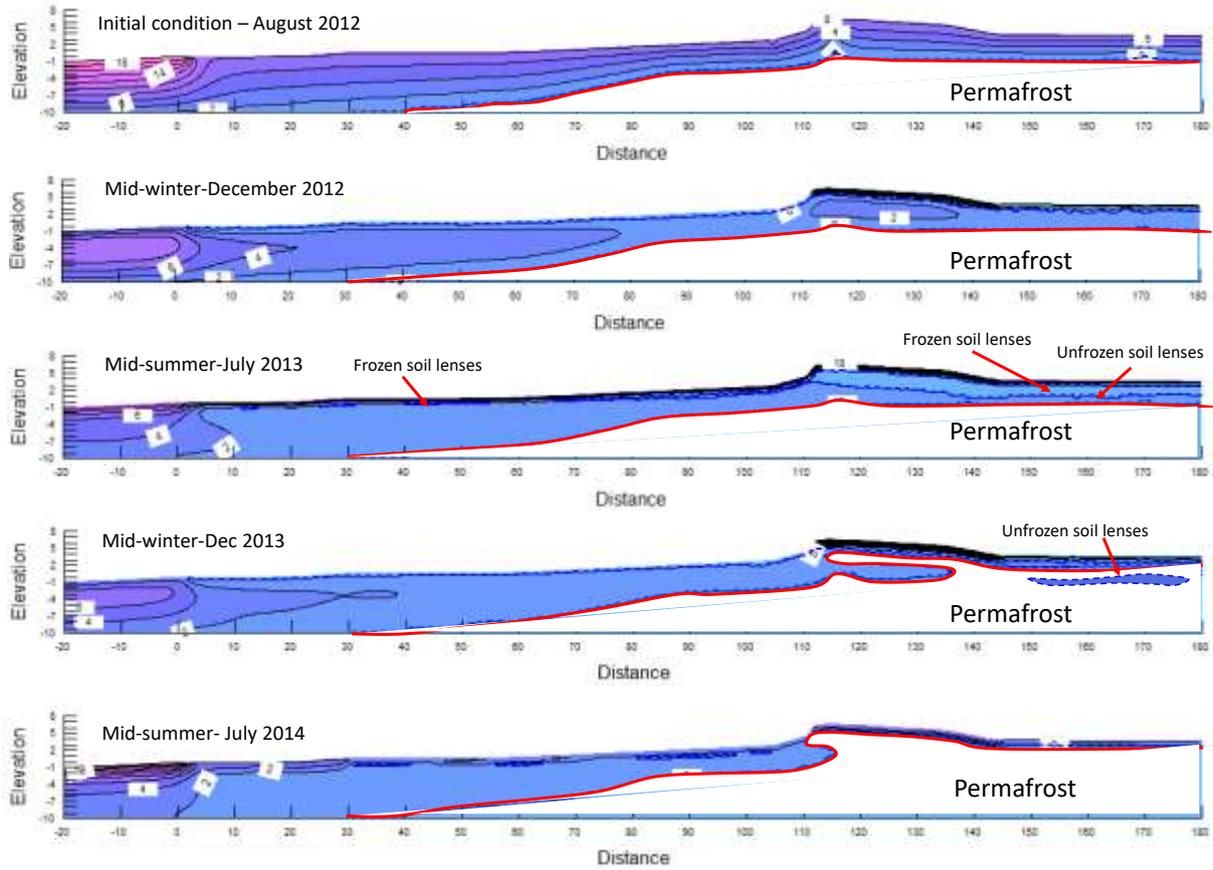

Figure 13: Thermal profile changes over time predicted by TEMP/W for the cross-section on Pesyakov Island. Red line shows the isoline at zero degree in each seasonal snapshot.

Figure 14 shows the comparison of the measured and predicted yearly trumpet curves and mean temperature curves for BH1, BH2 and BH3 (from their corresponding 1D models), while Figure 15 shows a similar comparison for BH4, BH5 and BH6 (from the 2D model). The trumpet

curves show the lowest and highest soil temperature at different depths over each monitored year. The trumpet curves together with the mean value are important to consider for design of structures on permafrost.

Both the 1D and 2D models predict well the first year of temperature variation (i.e. August 2012–August 2013) (Figure 14). The consistency between predicted and measured curves is considerably better for 2012–2013 than 2013–2014 at all boreholes. Note that there is only one year of measurement available for BH1 on the laida as the thermistor string was damaged in the second year.

The decrease in consistency between the predicted and the measured temperature in the second year is due to the assumed initial and boundary conditions. The initial temperatures at different depths were calibrated with the first temperature measurements, hence the prediction fits the measurement perfectly in August 2012. Over time, the predicted temperature fluctuates around the measured temperature with a certain deviation due to various uncertainties (e.g., soil spatial variability, measurement errors, model errors, etc). The predicted trumpet curves and mean temperature curves for 2013–2014 are generally sufficiently close to the measured curves for practical purpose.
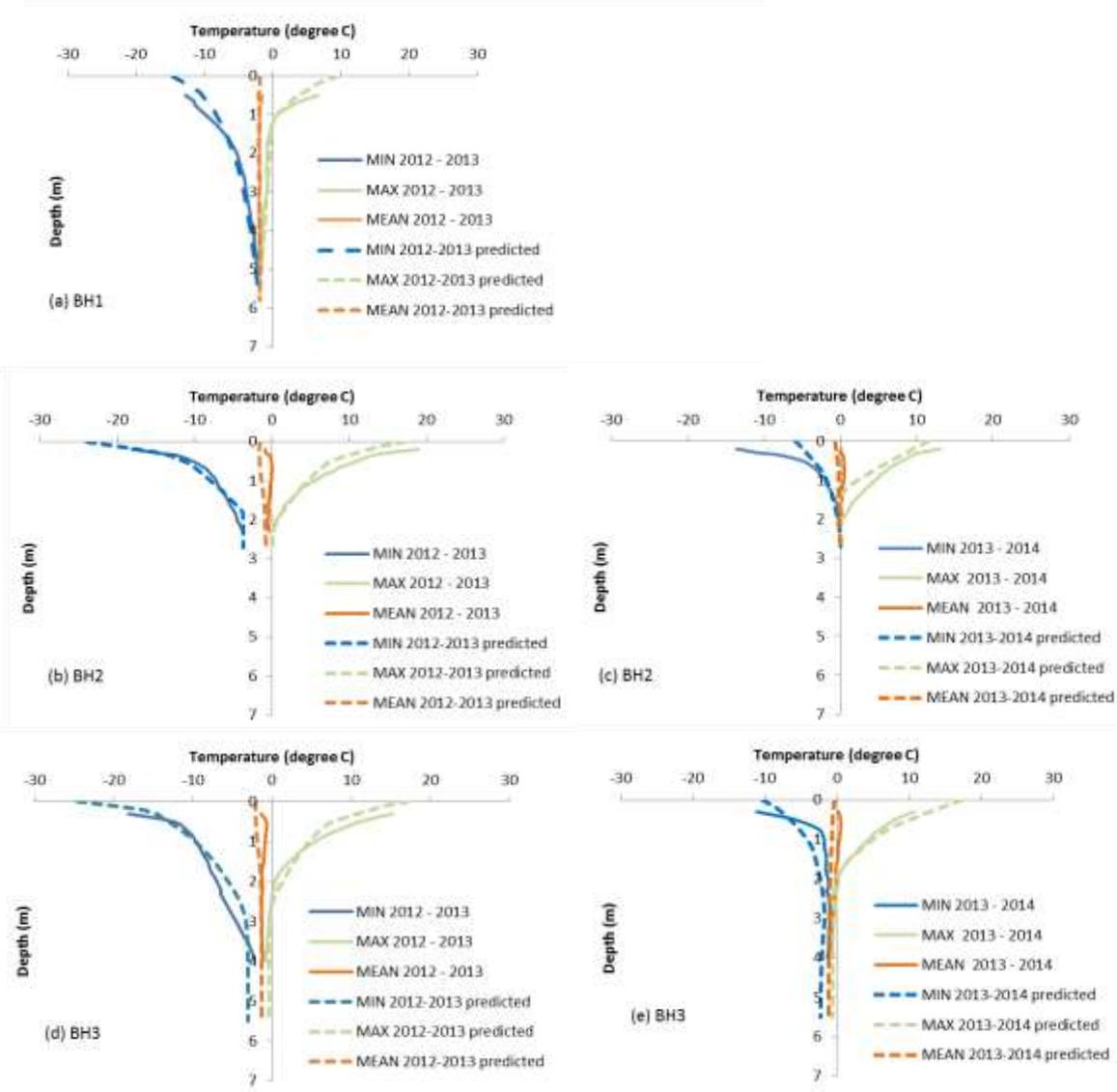
Figure 14: Measured and predicted trumpet curves for BH1, BH2 and BH3 from 1D models.
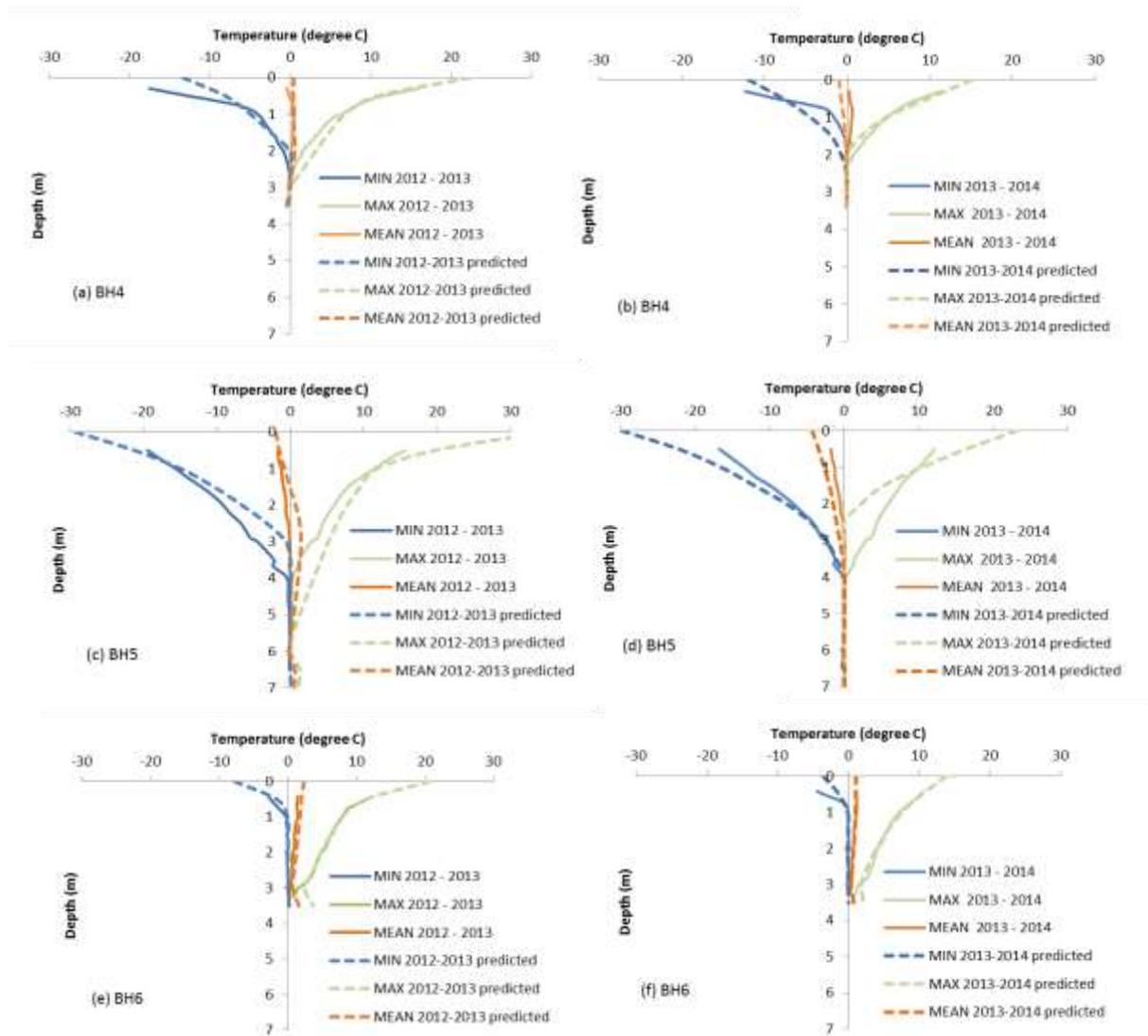
Figure 15: Measured and predicted trumpet curves for BH4, BH5 and BH6 from the 2D model

4   Conclusions

Analyses of soil temperature variation at six boreholes located in different geomorphological settings over two continuous years shows that the response of ground temperature to air temperature depends significantly on the insulation provided by the snow and grass cover as well as the topsoil properties. During winter, the conduction of latent heat at some locations (e.g. at the toe of the bluff) can be impeded considerably by the build-up of a snowbank before the ground surface becomes fully frozen. The ground temperature can therefore remain just below zero over the whole winter, even when the air temperature drops into the negative range.

Conversely, at locations where the snow and grass cover is thin (e.g. top of the bluff), the ground temperature follows closely the variation of the air temperature over the whole winter. The reduction of ground temperature relative to air temperature increases at locations having increasing snow and grass cover. In summer, the ground temperatures at all locations reflect quite closely the variation in air temperature as there is no influence from snow cover. The surface cover also contributes to reducing magnitude and to delaying the variation of the soil temperatures relative to the air temperature. These factors must be taken into account in constructing a thermal model for permafrost soils.

Numerical models of the thermal variation over the two years studied show the seasonal migration and retreat of the permafrost table and reflect the complexity of the thermal regime at the site. The numerical results explain the formation of frozen soil lenses/layers within a thawed soil mass and unfrozen soil lenses/layers within a frozen soil mass, which is important to take into account when investigating and constructing in regions affected by permafrost. The results from the numerical model can be employed for future evaluation, assessment and design of infrastructure on permafrost in Varandey settlement or similar regions. The study provides a useful tool and reference for the design of field investigations with respect to, for example, borehole locations, number of boreholes and thermistor string depth.

5 Acknowledgement:

6 References

AARI. 2016. Barents Sea. URL: http://www.aari.ru/resources/a0013_17/barents/atlas_barents_sea/_Atlas_Barenc_Sea_seasons/text/Barenc.htm#2p6.1. Accessed: 01.Dec.2017

Andersland, O.B. & Ladanyi, B. 2004. Frozen Ground Engineering. John Wiley & Sons.

ASABE. 2017. Typical soil properties. URL: https://elibrary.asabe.org/. Accessed: 29.Oct.2017

CALM. 2017. The Circumpolar Active Layer Monitoring Network-CALM: Long-Term Observations of the Climate-Active Layer-Permafrost System. URL: https://www2.gwu.edu/~calm/. Accessed: 01. Nov. 2017

Farouki, O.T. 1981. *Thermal properties of soils.* United States Army Corps Of Engineers, Cold Regions Research and Engineering Laboratory.

Flynn, D., Kurz, D., Alfaro, M. & Graham, J. 2016. Forecasting Ground Temperatures under a Highway Embankment on Degrading Permafrost. Journal of Cold Regions Engineering, **30**.

Fritz, M., Vonk, J.E. & Lantuit, H. 2017. Collapsing Arctic coastlines. Nature Clim. Change, **7**, 6-7, doi: 10.1038/nclimate3188.

GEO-SLOPE. 2012. *Thermal Modeling with TEMP/W: An Engineering Methodology.* GEO-SLOPE International Ltd.

GEOPRECISION GmbH. 2016. Thermistor string. URL: http://www.thermistor-string.com/. Accessed: 01.Mar.2016

Goering, D.J. 2003. Thermal Response of Air Convective Embankments to Ambient Temperature Fluctuations. *In*: Phillips, M., Springman, S. & Arenson, S.M. (eds.) *Eighth international Conference on Permafrost*. Balkema, Lisse, Zurich, Switzerland, 291-296.

Gubarkov, A.A., Khomutov, A.V. & Leibman, M.O. 2009. Contribution of lateral thermoerosion and thermodenudation to the coastal retreat at Yugorsky Peninsula, Russia. *Proceedings of the EGU General Assembly. 19-24 . Apr. 2009*, Vienna, Austria, 1785.

Guégan, E., Sinitsyn, A., Kokin, O. & Ogorodov, S. 2016. Coastal Geomorphology and Ground Thermal Regime of the Varandey Area, Northern Russia. Journal of Coastal Research, 1025-1031, doi: 10.2112/JCOASTRES-D-15-00147.1.

Guégan, E.B.M. & Christiansen, H.H. 2016. Seasonal Arctic Coastal Bluff Dynamics in Adventfjorden, Svalbard. Permafrost and Periglacial Processes, **27**, doi: 10.1002/ppp.1891.

Guglielmin, M. 2006. Ground Surface Temperature (GST), Active Layer and Permafrost Monitoring in Continental Antarctica. Permafrost and Periglac. Process., **17**, 133-143.

Harris, S.A., French, H.M., Heginbottom, J.A., Johnston, G.H., Ladanyi, B., Sego, D.C. & van Everdingen, R.O. 1988. Glossary of Permafrost and Related Ground-Ice terms. Technical Momorandum No. 142. International Permafrost Association, Terminology Working Group, Canada.

Heuer, C.F., Krzewinski, T.G. & Metz, M.C. 1982. Special thermal design to prevent thaw settlement and liquefaction. *In*: French, H.M. (ed.) *4th Canadian Conference on Permafrost*. National Research Council og Canada, Ottawa, Calgary, Alberta, 407-522.

Ivanova, N.V., Rivkin, F.M. & Vlasova, U.V. 2008. Stroyeniye i zakonomernosti formirovaniya kriogennoy tolshchi na poberezh'ye pechorskogo morya. [The permafrost structure and formation regularities on the pechora sea coast.]. Kriosfera Zemli [Earth's Cryosphere], **7**, 19.

Jones, B.M., Arp, C.D., Jorgenson, M.T., Hinkel, K.M., Schmutz, J.A. & Flint, P.L. 2009. Increase in the rate and uniformity of coastline erosion in Arctic Alaska. Geophysical Research Letters, **36**, doi: 10.1029/2008GL036205.

Kersten, M.S. 1949. *Laboratory research for the determination of thermal properties of soils.* University of Minnesota. Engineering Experiment Station and United States. Army. Corps of Engineers. St. Paul District.

Kristensen, L., Christiansen, H.H. & Caline, F. 2008. Temperatures in Coastal Permafrost in the Svea Area, Svalbard. *9th International Conference on Permafrost*. University of Alaska, Fairbanks, Fairbanks, Alaska, 1005-1010.

Novikov, V.N. & Fedorova, E.V. 1989. Destruction of coasts in the southern Barents Sea (in Russian). Vestnik MGU, 5, Geografiya, **1**, 64-68.

Ogorodov, S.A. 2004. Morpholitodynamics of coastal zone of Varandey area in Pechora sea under man-made impact (in Russian). Geoecology, Engineering Geology, Hydrogeology, Geocryology, **3**, 1-6.

Ogorodov, S.A. 2005. Human impacts on coastal stability in the Pechora Sea. Geo-Marine Letters, **25**, 190.

Ogorodov, S.A., Kokin, O.V., Sinitsyn, A.O., Guegan, E., Rodionov, I.V., Udalov, L.E., Kuznetsov, D.E., Likutov, P.E. & Kondratieva, S.T. 2014. *Research on dynamics of coastal zone of Barents and Kara seas in a changing arctic climate.* Federal State Budgetary Institution - N.N.Zubov State Oceanographic Institute.

Ostercamp, T.E. 2003. Establishing Long-term Permafrost Observatories for Active-layer and Permafrost Investigations in Alaska: 1977–2002. Permafrost and Periglac. Process., **14**, 331-342.

Raspisaniye Pogodi Ltd. 2016. Weather for 243 countries of the world. URL: http://rp5.ru/Weather_in_the_world. Accessed: 1.Jan.2015

Sinitsyn, A., Guegan, E., Kokin, O., Shabanova, N. & Ogorodov, S. 2017. A 50-years story on coastal erosion and hydrometeorological parameters in the Varandey area, Barents Sea (under revision). Coastal Engineering.

Thermal regime of permafrost at Varandey Settlement along the Barents Sea Coast, North West Arctic Russia

Highlights:

- Six boreholes were sampled along a 500 m horizontal cross-section
- Ground temperatures were monitored over two continous years
- The surface cover strongly influences the correlation between air and ground temperature
- Numerical models reveal formations of discrete frozen and unfrozen soil lenses